PROCEEDINGS, 45th Workshop on Geothermal Reservoir Engineering
Stanford University, Stanford, California, February 10-12, 2020
SGP-TR-216

Heterogeneous Hydrolysis of a Thermally Degrading Tracer

Jay T. Bender[1], Adam J. Hawkins[2], Robert D. Grooms, Colette J. Schissel, and Jefferson W. Tester

Smith School of Chemical and Biomolecular Engineering, Cornell University, Ithaca, NY 14853

jtb239@cornell.edu[1] | ajh338@cornell.edu[2]

Keywords: Reactive tracers, Thermal degradation, Thermal drawdown, Temperature sensing, Reservoir characterization, Geochemistry.

ABSTRACT

A major obstacle in commercializing geothermal resources is predicting the potential for cooling of production wells, particularly in the presence of cold water reinjection. Thermally degrading tracers such as phenyl acetate may enable advanced warning of "premature thermal breakthrough" if compounds with appropriate and known temperature-dependent reaction kinetics can be identified. This work investigates the potential for accelerated reaction rates in the presence of mineral surfaces (i.e., a heterogeneous reaction path). First, a homogeneous aqueous solution buffered with citric acid and sodium phosphate dibasic was spiked with phenyl acetate and the hydrolysis reaction was measured by spectrophotometry at room temperature. We then performed heterogeneous experiments with silica beads and coarse sand in a packed-bed reactor. After submerging the silica beads and coarse sand particles for several weeks, the measured reaction kinetics suggested that the rate constant increased after fluid-mineral contact had been established for several days. This could suggest a rate-limited surface maturation process to describe this time-dependency.

1. INTRODUCTION

Significant progress has been made with both the technological development and deployment of intermittent renewable energy sources such as wind and solar. However, intermittent renewables create utility challenges with peak supply periods missing peak demand periods introducing volatility to the energy market that needs predictability (Mason, 2010). Geothermal energy systems offer a complementary approach that does not require storage. Geothermal systems can be operated continuously providing baseload power that can help stabilize electricity markets with large contributions of intermittent renewables. Additionally, the thermal energy contained in a geothermal resource can be used to directly heat buildings and provide hot water in district energy systems (Fox et al., 2011).

Subsurface reinjection of produced fluids is widely employed to maintain production well fluid pressure and flow rates while also allowing for wastewater disposal (Horne, 1982). However, a significant number of geothermal power plants that utilize reinjection have experienced early temperature declines due to insufficient heat transfer surface area between injectors and producers (e.g., Horne, 1985; Stefánsson, 1997; Diaz et al., 2016; etc.). This behavior is known to result when inlet-outlet "short-circuiting" disrupts the spatial distribution of fluid flow and focuses fluids through narrow regions of high permeability (e.g., Hawkins et al., 2017a, 2017b, 2018).

Therefore, a major challenge in large-scale development of low-grade resources is to develop reservoir characterization methods capable of monitoring the progression of a cold front before it causes thermal drawdown of produced fluids extracted from the reservoir. Currently, observation wells can be used to monitor this progression, however these wells are expensive and may not be positioned in the low-impedance flow path (e.g., Hirtz, 2001; Lukawski et al., 2014; etc.). In addition, computational modeling can provide predictions of thermal breakthrough, but it is difficult to calibrate these models due to the complexity of subsurface flows. For geothermal energy wells to be economically viable, *in-operando* well temperature maintenance tools must be developed.

Early work at the Fenton Hill Hot Dry Rock (HDR) experimental reservoir suggested the progression of a thermal front could be monitored via the temperature-dependent kinetics of a thermally degrading (i.e., "reactive") tracer (e.g., Robinson and Tester, 1986, 1990; Robinson et al., 1988; etc.). Since then, only a limited number of thermally degrading tracer tests have been performed in commercial-scale geothermal reservoirs. Unfortunately, none of these trials had sufficient experimental resolution to determine the accuracy of estimates derived from these tests (e.g., Adams and Davis, 1991; Behrens et al., 2009; Du Teaux and Callahan, 1996; Kwakwa, 1988; Rose and Clausen, 2015).

Recent work by Hawkins et al. (2017a) demonstrated the use of thermally degrading tracers at a meso-scale site known as the "Altona Field Laboratory, (AFL)." At this spatiotemporal scale, experiments could be completed within a number of days as opposed to the commercial-scale which requires years or even decades to evaluate experimental tracers. A series of four reactive tracer tests conducted during six days of continuous hot water circulation through a cold, shallow fracture revealed progressively increased reaction rates. Interpretation of the results based on the temperature-dependent Arrhenius rate equation (Nottebohm et al., 2012) demonstrated that the thermally degrading tracer provided reasonable indication of reservoir heating. However, the absolute values of these temperature estimates deviated from measured temperatures by roughly 70 to 80 °C indicating that the rate constant values reported by Nottebohm and coworkers were not applicable to the Altona field application. Here, we perform packed-bed column experiments at the laboratory scale to investigate the potential catalytic effect of silica surfaces on thermally degrading tracers. These results are compared to a homogeneous batch experiment as well as the measured reaction rates at the Altona site.

2. METHODS

The reactive tracer tests performed at the AFL utilized phenyl acetate as a thermally degrading tracer. This carboxylic ester experiences base-catalyzed hydrolysis at near-neutral pH with relatively rapid kinetics suitable for the low-temperature conditions at the AFL (~10-74 °C). These field tests introduced an inert reference tracer simultaneously with the thermally degrading tracer to provide a conservative estimate of transport for comparison. Similarly, the experiments described here include the same inert reference tracer (the "C-Dot" nanoparticle) and phenyl acetate (Hawkins et al., 2017a). In the sub-sections below, phenyl acetate and the hydrolysis reaction is described in detail followed by a description of the temperature-dependent Arrhenius equation, the experimental setup, and the one-dimensional transport model used to convert measured tracer breakthrough curves to a first-order reaction rate.

2.1 Hydrolysis of Phenyl Acetate

Nottebohm et al. (2012) suggested the use of carboxylic esters as a thermally degrading tracer for characterizing subsurface reservoir temperatures. Phenyl acetate, for example, undergoes a rapid, temperature-dependent hydrolysis reaction at relatively low temperatures (10 to 80 °C). This range of temperature dependency made the use of phenyl acetate as a thermally degrading tracer appropriate for the conditions at the meso-scale Altona Field Laboratory (Hawkins et al., 2017a). This hydrolysis reaction (Figure 1) follows a (pseudo-) first order reaction and the temperature-dependency of its rate constant, k, is governed by the Arrhenius law such that $k = A\exp(-E_a/RT)$, where A, E_a, R, and T are the pre-exponential factor, activation energy, universal gas constant, and absolute temperature, respectively.

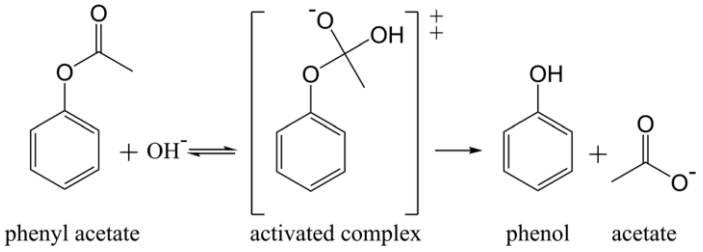

Figure 1: Overall reaction mechanism for the base-catalyzed hydrolysis of phenyl acetate. Phenyl acetate hydrolyzes to form products phenol and acetate. The first step of this mechanism is rate-limiting and the final phenol and acetate products are in equilibrium.

Under homogeneous conditions, the (pseudo-) first-order reaction is described as

$$\frac{d}{dt}[\mathrm{PhAc}] = -k_b[\mathrm{PhAc}][\mathrm{OH}^-], \tag{1}$$

where k_b is the bulk reaction rate constant and [PhAc] and [OH^-] are the concentrations of phenyl acetate and the hydroxide ion, respectively. Assuming the concentration of the hydroxide ion is much larger than the other species allows one to incorporate the [OH^-] term as a constant. Thus, an intrinsic rate constant, k_i, can be defined as the product of k_b and [OH^-]. Under heterogeneous conditions, the bulk rate constant is equal to the intrinsic rate constant added to the product of the catalytic rate constant, k_c, and the surface concentration of [OH^-] such that Equation 1 becomes

$$\frac{d}{dt}[\mathrm{PhAc}] = -(k_i + k_c)[\mathrm{PhAc}]. \tag{2}$$

To determine the value of the bulk rate constant, the transient reduction of reactant concentration, C, starting at an initial concentration, C_0, is measured as a function of time. For a first-order reaction, a plot of the logarithm of normalized concentration (C/C_0) vs. elapsed reaction time gives a linear function and the slope of this line is equivalent in magnitude to k_b.

Because of the rapid reaction rates anticipated for phenyl acetate hydrolysis, rapid analysis of reaction concentrations had to be performed to obtain sufficient resolution of the kinetics. A fluorescence spectrophotometer (Cary Eclipse, Agilent Technologies) allowed for these rapid measurements to be performed. However, only the reaction product (phenol) can be measured via fluorescence so determination of reactant concentration (phenyl acetate) relied on the assumption of full conversion of phenyl acetate to phenol.

2.2 Experimental Setup

2.2.1 Buffer Solution

Both the homogeneous and heterogeneous experiments utilized a buffer solution to prevent significant fluctuations in pH. The buffer was composed of citric acid and sodium phosphate dibasic known as a McIlvaine buffer. This buffer solution was picked because solutions with pH values ranging from 2.2 to 8.0 can be easily made with inexpensive chemicals (McIlvaine, 1921). It was assumed that ions from the buffer solution did not influence the kinetics of the base-catalyzed hydrolysis reaction. Finally, to control fluctuating dissolved oxygen, nitrogen was bubbled through the buffer solutions.

2.2.2 Batch Reactor

A Cary Eclipse Fluorescence Spectrophotometer equipped with a fiber-optic probe both from Agilent Technologies measured phenol concentration as a function of time in a sealed batch reactor (Thermo-Scientific, model number NESLAB RTE 10) (Figure 2). To initiate a kinetics experiment, 2.89E-6 kg of phenyl acetate dissolved in warm citric acid was included within a total volume of 200E-6 m^3 of

deoxygenated buffer in the reaction chamber (Figure 2c) After full conversion of phenyl acetate to phenol, the final phenol concentration is 9.99E-3 kg/m^3. Warm citric acid was chosen for the solvent of phenyl acetate because the acidic pH value of the citric acid solution avoided any base-catalyzed phenyl acetate hydrolysis prior to the start of the experiment and because phenyl acetate is immiscible in water. The spectrophotometer measured concentration of phenol, the reaction product, was measured continuously every 10 seconds throughout each experiment. The concentration of reactant, phenyl acetate, was measured assuming mass balance.

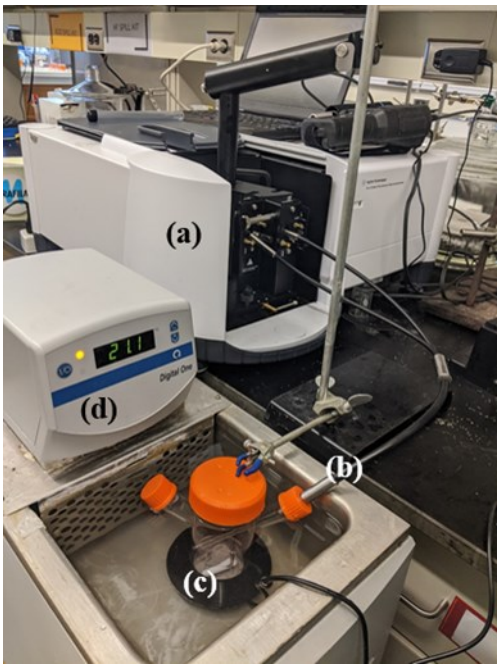

Figure 2: Schematic of the homogeneous experimental apparatus including (a) a Cary Eclipse Fluorescence Spectrophotometer from Agilent Technologies; (b) a fiber-optic probe for measuring phenol concentration; (c) a sealed reaction vessel that is stirred with a magnetic stir bar; (d) a water bath for controlling the temperature in the reaction vessel.

2.2.3 Packed-bed Column Experiments

The packed-bed column experiments (Figure 3) included two different silica-dominated substrates. Four experiments were performed using Pyrex amorphous silica glass beads manufactured by Corning Inc. (lot number 13916999) and purchased from Krackeler Scientific (catalog number 5663H29) with a mean radius of 1.5 mm. Two further experiments were performed using coarse-grained silica sand from Unimin with a mean radius of radius of 0.45 mm (Day et al., 2020). To evaluate the potential for a slowly-developing catalytic surface, repeat column tests were performed under varying solid-fluid contact time. For the two silica sand experiments, the first experiment was performed immediately after filling the column with sand and water and the second experiment was performed after 14 d of constant solid-fluid contact or “maturation” time. For the four glass bead experiments, column tests were performed after 0, 5, 32, and 42 d.

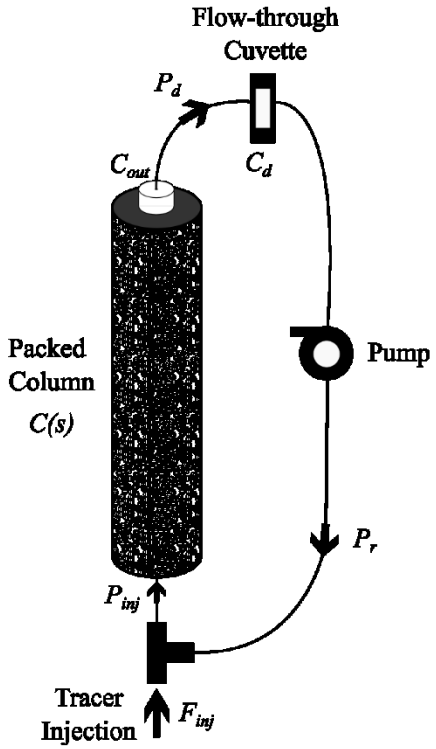

Figure 3: Schematic representation of tracer and fluid transport through the packed column reaction system. Tracer is injected into the system by the input function F_{inj} at flow rate equal to Q. The initial injectate is delayed by pipeline delay function P_{inj} before flowing into the packed column. The packed column effluent is delayed by pipeline delay function P_d before flowing into the detector. Finally, the detector effluent is delayed by pipeline delay function P_r before being recirculated back through the packed column.

For heterogeneous experiments, the increase in phenol (reaction product) was measured using a continuous flow-through cuvette system that allowed for measurement of phenol by spectrophotometry in real-time. Produced column effluent recirculated into the column inlet to ensure each experiment could be running long enough for the reaction to reach completion. A pump manufactured by Eldex (Model A-10-S) provided continuous fluid circulation for up to 2 d.

Tracer injectate consisted of 2.39E-8 kg of C-Dots and 3.46E-7 kg of phenyl acetate (equivalent to 2.49E-7 kg of phenol). Both tracers were dissolved in 1E-6 m^3 of buffered solution at a pH of roughly 6.3 to 6.4 resulting in an injection concentration of 23.9 ppm of C-Dots and 345.6 ppm phenyl acetate (equivalent to 239.0 ppm phenol). The Cary Eclipse equipped with a flow-through cuvette (Figure 3) measured effluent concentration at the detector, C_d, every 20 s throughout each experiment. The Cary Eclipse equipped with a flow-through cuvette (Figure 3) measured effluent concentration at the detector, C_d, every 20 s throughout each experiment. Tracer injection began at an elapsed time of 0 s and finished within roughly 60 s.

2.3 Transport Model for Packed-Bed Column Tests

The bulk reaction rate constant, k_b, was determined using the reactive transport model presented in Hawkins et al. (2017a). The model is adapted here for a packed-bed column whereas the original formulation considered a discrete rock fracture. Advection and dispersion occur in the fluid-filled pore spaces of the granular media in the direction of the velocity vector (Figure 3) and a first-order rate constant is introduced to model the hydrolysis reaction. Adsorption and matrix diffusion are considered in the form presented in Hawkins et al. (2017a), but these are negligible for the present study. The governing equation is

$$\frac{\partial C}{\partial t} = D\frac{\partial^2 C}{\partial x^2} - v\frac{\partial C}{\partial x} - k_b C, \tag{3}$$

where D, v, and C are the dispersion coefficient, mean fluid velocity in the pore spaces, and tracer concentration, respectively. From Hawkins et al. (2017), tracer concentration, C, eluted from the fluid volume of the porous media, V_f ($V_f = Qx/v$), is given in Laplace space as

$$C(s) = \exp\left[\frac{Pe}{2}\left(1 - \sqrt{1 + \frac{4\,(k_b+s)\,V_f}{Q\,Pe}}\right)\right], \tag{4}$$

where Pe is the dispersional Peclet number ($Pe = (vx)/D$), s is the Laplace transform variable, and Q is the volumetric flow rate ($Q = V_f v/x$) circulated through the porous media. To model the measured concentrations of the two tracers, Pe and k_b were treated as unknowns

solved by the non-linear conjugate gradient method and the objective function calculated the residual norm of least-square error. In addition, slight adjustments to V_f were allowed to account for potential errors in measurement of the porous fluid volume.

Several transfer functions are introduced here to account for pipeline delays and a non-instantaneous input of tracer. A mass of tracer, M_{inj}, dissolved in a finite volume of injectate, V_{inj}, is modeled in Laplace space as

$$F_{inj} = \frac{1}{s}\frac{M_{inj}}{V_{inj}}\left(1 - \exp\left(-s\frac{V_{inj}}{Q}\right)\right). \quad (5)$$

Circulating fluids experienced pipeline delays when they were transported from the packed column outlet to the detector inlet and from the detector outlet back to the packed column inlet (Figure 3). In addition, the initial injection of tracers experienced a pipeline. These delays were accounted for by a transfer function of the form

$$P(s) = \exp(-t_d s) \quad (6)$$

where t_d is the delay time (sec) (Reimus et al., 2003). The measured concentration detected, C_d, at the flow-through cuvette is then modeled as

$$C_d(s) = \frac{C\,F_{inj}\,P_{inj}\,P_d}{1 - C\,P_d\,P_r}, \quad (7)$$

where P_{inj} models pipeline delays due to injection plumbing, P_d models pipeline delays between the column effluent and the detector, and P_r models the influence of tracer recirculation through the closed system. A MATLAB® script provided in Hollenbeck (1998) numerically inverted the convoluted Laplace transform represented by Equation 7 to solve for concentration in space and time. Figure 3 shows a schematic of the transfer functions used to account for tracer recirculation. Note that the reaction rate constant in the recirculation system is assumed negligible relative to the bulk rate constant experienced in the packed-bed.

3. RESULTS

The homogeneous experiment ran continuously for six. After 1.9 d the normalized reactant concentration (C/C_0) reached 0.5 (Figure 4). A linear fit to the measured data suggests an intrinsic reaction rate, k_i, for the homogeneous room temperature experiment is 5.36E-6 s^{-1}. The measured dissolved oxygen at the beginning of the experiment was 9.3%, but rose to 98% by the end of the experiment. The starting and final pH were 6.34 and 6.30, respectively.

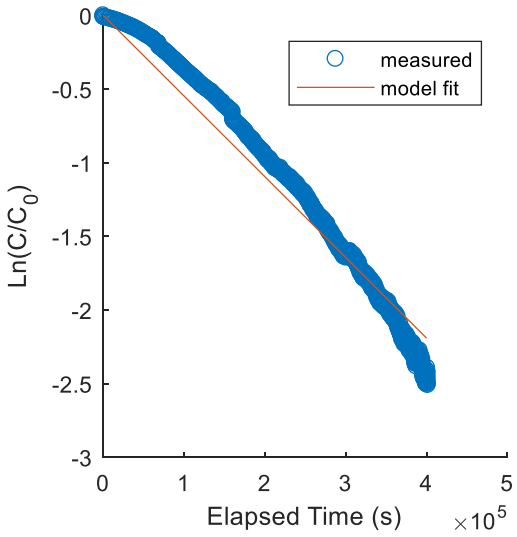

Figure 4: Plot of normalized reactant concentration (phenyl acetate) as a function of elapsed time. The model fit represents the best-fit match to measured concentrations using a linear model with a y-intercept of zero. The absolute value of the slope is equal to the intrinsic rate constant, k_i.

The four heterogeneous experiments with glass beads ran for roughly 2 d (Figure 5). By 0.3 d the normalized concentration of the reaction product, γ_{Ph}, (phenol) reached a steady-state value of one. This normalized concentration is calculated as $\gamma_p = C_{Ph}V_{sys}/M_{inj}$, where C_{Ph} is the measured concentration of phenol and V_{sys} is equal to the total volume of the circulation system including the pore fluids and the recirculation system. Therefore, a normalized value of one indicates that the total mass injected has been fully diluted in the total system volume. Using the best-fit model (Equation 7), the bulk rate constant, k_b, after 0, 5, 32, and 42 d of solid-fluid contact time were 1.21E-4, 1.40E-4, 1.56E-4, and 1.61E-4, respectively (Table 1). The range of best-fit values for the Peclet number, Pe, and pore fluid volume, V_f, were 15-41 and 32.9E-6-43.9E-6 m^3, respectively. Measured pH at the beginning of the column tests for all four experiments was 6.3 and dissolved oxygen ranged from 4.5% to 14%.

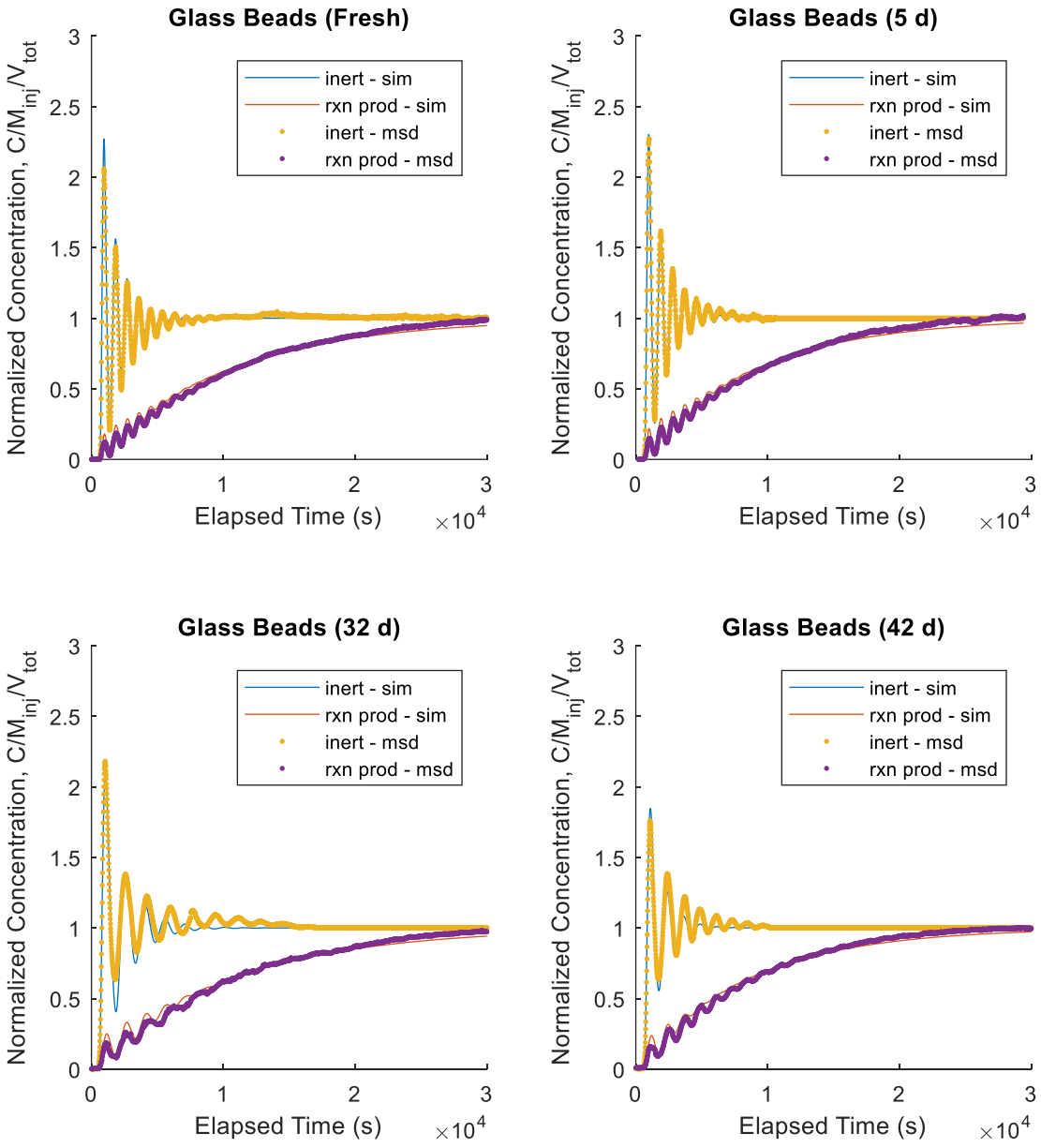

Figure 5: Measured and simulated tracer breakthrough curves for freshly saturated glass beads (top-left) and after 5 d (top-right), 32 d (bottom-left), and 42 d (bottom-right) of solid-fluid contact time. Model fits solved for pore-fluid volume, the dispersional Peclet number, and the reaction rate constant.

Table 1: Summary of results from homogeneous and heterogeneous base-catalyzed phenyl acetate hydrolysis experiments and best-fit parameters

Matrix	Temperature (°C)	pH	Dissolved Oxygen (% saturated)	Bulk Rate Constant, k_b (s^{-1})	Reaction Half-life (h)	Pore Fluid Volume, V_f (m^3)	Peclet Number, Pe (-)	[5]Geometric Surface Area (m^2)
[1]Homogeneous	20.8	~6.5	N/A	3.59E-7	536	n/a	n/a	n/a
Homogeneous	20.8	6.3	9.3%	5.48E-6	35	n/a	n/a	n/a
[2]Fresh Sand	20.8	6.4	10.4%	1.32E-4	1.46	17.5E-6	23	0.58
Aged Sand (14 d)	20.8	6.3	13.5%	1.57E-4	1.23	17.3E-6	46	0.58
[3]Glass Beads (fresh)	20.8	6.3	6.6%	1.21E-4	1.59	32.9E-6	38	0.14
Glass Beads (5 d)	20.8	6.3	4.5%	1.40E-4	1.38	34.3E-6	41	0.14
Glass Beads (32 d)	20.8	6.3	14%	1.56E-4	1.24	43.0E-6	15	0.12
Glass Beads (42 d)	20.8	6.3	6.7%	1.61E-4	1.20	43.9E-6	19	0.12
[4]Altona Field Tests	20.8	6.4	0%	1.29E-4	1.5	82.4E-3	35	28.3

[1]based on the average of two values reported in Nottebohm et al. (2012) determined for pH = 6 and pH = 7
[2]mean radius of coarse-grained sand is 0.45 mm (May et al., 2020)
[3]mean radius of silica glass beads is 1.5 mm (Gu, 2018)
[4]area, volume, and Peclet number from Hawkins et al. (2018) and reaction rate constant and pH from Hawkins et al. (2017a).
[5]geometric surface area, A_s, calculated as $A_s = (3/r_g)(V_{col} - V_f)$, where r_g is the single-grain radius and V_{col} is the volume of the column (104.4E-6 m^3)

For the two heterogeneous experiments with coarse-grained silica sand, the first experiment (0 d of solid-fluid contact time) ran for roughly 2 d and the second experiment (14 d of contact time) ran for roughly 1 d (Figure 6). The volumetric flow rate during the first experiment was 5.71E-9 m^3s^{-1} whereas the volumetric flow rate during the second experiment was identical to the four glass bead experiments (4.60E-8 m^3s^{-1}). The best-fit model to measured data suggests that Pe and V_f for the first experiment is 23 and 17.5E-6 m^3, respectively and 46 and 17.3E-6 m^3 for the second experiment. After 14 d of solid-fluid contact time, k_b rose from 1.32E-4 s^{-1} to 1.57 s^{-1}. Measured pH at the beginning of the column tests ranged from 6.3 to 6.4 and dissolved oxygen ranged from 10.4% to 13.5%.

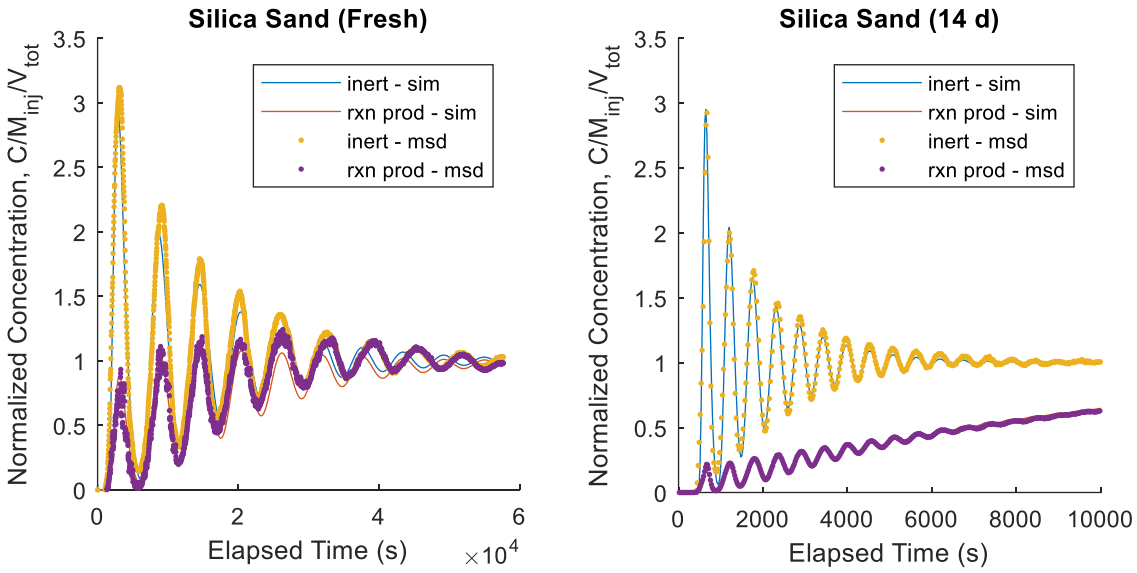

Figure 6: Measured and simulated tracer breakthrough curves for freshly coarse-grained silica sand (left) and after 14 d (right) of solid-fluid contact time. Model fits solved for pore-fluid volume, the dispersional Peclet number, and the reaction rate constant. Note that volumetric flow rate, Q, for fresh sand and 14 d sand were 5.71E-9 and 4.60E-8 m^3s^{-1}, respectively.

4. DISCUSSION AND CONCLUSIONS

The experiments described here reveal accelerated reaction kinetics of an organic compound in contact with silica surfaces. The bulk reaction rate of phenyl acetate hydrolysis is roughly a factor of 30 larger than the intrinsic rate constant under homogeneous conditions found here and roughly a factor of 450 larger than previously reported in the kinetics literature. In packed-bed column experiments, the bulk reaction rate across six experiments ranged from 1.21E-4 to 1.61E-4 s^{-1}. Of the six experiments, four of them were performed with a column filled with amorphous silica glass beads and the other two columns were filled with coarse-grained silica sand. Under homogeneous reaction conditions, the intrinsic reaction rate constant is 5.48E-6 s^{-1}.

A slight increase in the bulk reaction rate appears to result from lengthening the solid-fluid contact time. Compare, for instance, the bulk reaction rate constant in the presence of glass beads during 42 d of solid-fluid contact time. When the reaction rate is measured immediately after filling the column with beads and aqueous solution, the bulk rate constant is 1.21E-4 s^{-1}. After "maturing" the beads for 5, 32, and 42 d, however, the reaction rate increases monotonically to 1.40E-4, 1.56E-4, and 1.61E-4 s^{-1}, respectively. In addition, this behavior is observed for the silica sand. After 14 d of solid-fluid contact time, the bulk rate constant for sand rises from 1.32E-4 to 1.57E-4 s^{-1}. This suggests that the mechanism responsible for the accelerated bulk reaction rate is time-dependent.

As discussed in the Introduction section, the lab experiments described here are motivated in the context of field tests performed at the meso-scale Altona Field Laboratory. There, the observed reaction rate of phenyl acetate hydrolysis at 20.8 °C was 1.29E-4 s^{-1}. This reaction rate is consistent with the range measured in the laboratory experiments presented here. This suggests that the apparent acceleration of phenyl acetate hydrolysis reported in Hawkins et al. (2017a) resulted from a heterogeneous reaction consisting of an intrinsic rate constant and a much larger catalytic rate constant induced by the solid-fluid interface.

Surprisingly, the increase in the bulk reaction rate appears to reach a limit as the active surface area for catalysis increases. Compare, for instance, the bulk rate in the presence of silica sand and glass beads. The packed-bed column filled with sand contains a total geometric surface area (assumes perfect spheres) of roughly 0.6 m^2 whereas a column filled with spherical glass beads contains a total geometric area of roughly 0.1 m^2. Even more dramatic, heat transfer experiments at Altona suggest that a surface area of roughly 28 m^2 provided a catalytic surface. Despite this two orders of magnitude difference in surface area, the bulk reaction rate constants for these three materials ranged, at most, from 1.29E-4 to 1.61E-4 s^{-1}. This may suggest that the dependency of the bulk rate constant rises asymptotically to a threshold rate as active surface area increases. Or, alternatively, this may suggest that the number of total active sites for catalysis is roughly equal across these three scenarios, although this is unlikely considering each material consists mostly of silica.

In the context of practical use of hydrolysis as a target reaction for selecting thermally degrading tracers, the results presented here suggest that subsurface mineralogy must be considered. As reported above, silica minerals can introduce a heterogeneous reaction capable of raising the bulk rate constants by nearly a factor of 30. Without considering this effect, the interpretation of a thermally degrading tracer test can dramatically over-estimate the mean subsurface temperature of a geothermal reservoir. This could lead to an unexpected drop in production well temperatures.

Future investigation of this apparent catalysis will focus on temperature-dependency and extended maturation times. Performing these column experiments at temperatures ranging from 10 to 80 °C will allow for determination of the Arrhenius parameters such that effective reservoir temperatures can be determined from the breakthrough curves of thermally degrading tracers. Extending the maturation times of the column media will allow for identification of the long-term development of the apparent catalysis. Additional investigation will also consider varying the active surface area for catalysis and further investigate the influence of dissolved oxygen on the reaction behavior.

5. ACKNOWLEDGEMENTS

This material is based upon work supported by the U.S. Department of Energy, Office of Energy Efficiency and Renewable Energy (EERE), Office of Technology Development, Geothermal Technologies Program, under award DE-EE0006764.

REFERENCES

Adams, M.C., and Davis, J.: Kinetics of fluorescein decay and its application as a geothermal tracer, *Geothermics*, **20**, (1991), 53-66.

Behrens, H., Ghergut, I., Sauter, M., and Licha, T.: Tracer properties and spiking results (from geothermal reservoirs), *Proceedings*, 34th Workshop on Geothermal Reservoir Engineering, Stanford University, Stanford, CA (2009).

Diaz, A.R., Kaya, E., and Zarrouk, S.J.: Reinjection in geothermal fields – A worldwide review update, *Renewable and Sustainable Energy Reviews*, **53**, (2016), 105-162.

Du Teaux, R.T., and Callahan, J.: Comparing reactive and non reactive tracers to measure changes in liquid dominated, fractured geothermal reservoirs, *Proceedings*, Annual Meeting of the Geothermal Resources Council, Portland, OR (1996).

Fox, D.B., Sutter, D., and Tester, J.W.: The thermal spectrum of low-temperature energy use in the United States, *Energy & Environmental Science*, **4**, (2011), 3731-3740.

Gu, X.: Hydrolysis Kinetics of Phenyl Acetate as a Reactive Tracer under Heterogeneous Conditions, *Master's Thesis*, Cornell University (2018).

Gu, X., Hawkins, A.J., and Tester, J.W.: Temperature-Dependent Kinetics of Phenyl Acetate Hydrolysis, *Proceedings*, 43rd Workshop on Geothermal Reservoir Engineering, Stanford University, Stanford, CA (2018).

Hawkins, A.J., Fox, D.B., Becker, M.W., and Tester, J.W.: Measurement and simulation of heat exchange in fractured bedrock using inert and thermally degrading tracers, *Water Resources Research*, **53**, (2017a), 1210-1230.

Hawkins, A.J., Becker, M.W., and Tester, J.W.: Inert and adsorptive tracer tests for field measurement of flow-wetted surface area, *Water Resources Research*, **54**, (2018), 5341-5358.

Hirtz, P.N., Kunzman, R.J., Broaddus, M.L., and Barbitta, J.A.: Developments in tracer flow testing for geothermal production engineering, *Geothermics*, **30**, (2001), 727-745.

Hollenbeck, K.J.: INVLAP.m: A MATLAB® function for numerical inversion of Laplace transforms by the de Hoog algorithm, (1998), Retrieved from http://www.isva.dtu.dk/staff/karl/invlap.htm

Horne, R.N.: Geothermal Reinjection Experience in Japan, *Society of Petroleum Engineers*, (1982).

Horne, R.N.: Reservoir engineering aspects of reinjection, *Geothermics*, **14**, (1985), 449-457.

Kwakwa, K.A.: Tracer measurements during long-term circulation of the Rosemanowes HDR geothermal system, *Proceedings*, 13th Workshop on Geothermal Reservoir Engineering, Stanford University, Stanford, CA (1988).

Lukawski, M.Z., et al.: Cost analysis of oil, gas, and geothermal well drilling, *Journal of Petroleum Science and Engineering*, **118**, (2014), 1-14.

Mason, I.G., Page, S.C., and Williamson, A.G.: A 100% renewable electricity generation system for New Zealand utilizing hydro, wind, geothermal and biomass resources, *Energy Policy*, **38** (2010), 3973-3984.

May, D.F., Hassanpour, B., Sinclair, L., Hawkins, A.J., and Cathles, L.M.: Hydrophobic adsorption of carbon nanoparticles in sand-packed columns, *submitted for peer-review* (2020).

McIlvaine T.C.: A buffer solution for colorimetric comparison, *Journal of Biological Chemistry,* **49**, (1921), 183-186.

Nottebohm, M., Licha, T., & Sauter, M. (2012). Tracer design for tracking thermal fronts in geothermal reservoirs, *Geothermics*, **43**, 37-44.

Reimus, P., Pohll, G., Mihevc, T., Chapman, J., Haga, M., Lyles, B., and Sanders, P.: Testing and parameterizing a conceptual model for solute transport in a fractured granite using multiple tracers in a forced-gradient test, *Water Resources Research*, **39**, (2003), 1-15.

Robinson, B.A., and Tester, J.W.: Characterization of flow maldistribution using inlet-outlet tracer techniques: An application of internal residence time distributions, *Chemical Engineering Science*, **41**, (1986), 469-483.

Robinson, B.A., and Tester, J.W.: Kinetics of alkaline hydrolysis of organic esters and amides in neutrally-buffered solution, *International Journal of Chemical Kinetics*, **22**, 431-448.

Robinson, B.A., Tester, J.W., and Brown, L.F.: Reservoir sizing using inert and chemically reacting tracers, *SPE Formation Evaluation*, **2**, (1988), 227-234.

Rose, P., and Clausen, S.: The use of Amino G as a thermally reactive tracer for geothermal applications, *Proceedings*, World Geothermal Congress, Melbourne, Australia (2015).